Effect of chromium doping on superconductivity and charge density wave order in the kagome metal $Cs(V_{1-x}Cr_x)_3Sb_5$

Gaofeng Ding,[1,2] Hongliang Wo,[1,2] Yiqing Gu,[1,2] Yimeng Gu,[1,2] and Jun Zhao[1,2,3,4,*]

[1]*State Key Laboratory of Surface Physics and Department of Physics, Fudan University, Shanghai 200433, China*

[2]*Shanghai Qi Zhi Institute, Shanghai 200232, China*

[3]*Institute of Nanoelectronics and Quantum Computing, Fudan University, Shanghai 200433, China*

[4]*Shanghai Research Center for Quantum Sciences, Shanghai 201315, China*

(Received 8 October 2022; accepted 8 December 2022; published 26 December 2022)

The recently discovered kagome metal AV_3Sb_5 (A = K, Rb, Cs) with intertwined superconductivity and charge density wave (CDW) order has attracted considerable interest. Here we investigate the evolution of CDW and superconductivity in $Cs(V_{1-x}Cr_x)_3Sb_5$, where chromium substitution for vanadium introduces extra electron carriers. Our experiments reveal that the CDW order is gradually suppressed under chromium doping, which can be understood from the band structure modifications induced by electron doping. This highlights the importance of the van Hove singularities near the M and L points for CDW instability. The anomalous Hall effect that is coupled with CDW in CsV_3Sb_5 only appears in lightly doped $Cs(V_{1-x}Cr_x)_3Sb_5$ and vanishes at $x \geqslant 0.06$ when the CDW order remains relatively strong. Unlike hole- and isovalent-doped AV_3Sb_5, where superconductivity is enhanced upon suppression of CDW, superconductivity is rapidly suppressed under chromium doping, pointing to a conventional s-wave pairing.

DOI: 10.1103/PhysRevB.106.235151

I. INTRODUCTION

The newly discovered kagome metal AV_3Sb_5 (A = K, Rb, Cs), where the vanadium ions form the ideal quasi-two-dimensional kagome nets, displays interesting phenomena, including nontrivial band topology, superconductivity, and charge density wave (CDW) order [1–6]. AV_3Sb_5 exhibits CDW order at $T_{CDW} = 78$ to 104 K, followed by superconductivity below $T_c = 0.92$ to 2.5 K [1–3]. Evidence for time-reversal symmetry breaking was revealed by scanning tunneling microscopy (STM) and muon spin relaxation in the CDW ordered state [7–10]. This was accompanied by the anomalous Hall effect (AHE) [11–13] with an absence of detectable local magnetic moments [1,14], which were suggested to be associated with a chiral CDW order [15–17]. Regarding the pairing symmetry of superconductivity, while early thermal conductivity measurements suggested nodal superconductivity [18], other measurements such as nuclear magnetic resonance spectroscopy, magnetic penetration depth, and STM on CsV_3Sb_5 indicated nodeless [19] and conventional s-wave pairing [19–22]. In addition, exotic correlation-driven experimental phenomena related to CDW and superconductivity, such as electronic nematicity [23,24] and possible Majorana zero modes [25], have also been observed. To understand these interesting phenomena, it is important to elucidate the nature of the CDW state and superconductivity, and their interplay.

Carrier doping effectively tunes Fermi surface instabilities, which can provide valuable insight into the mechanism behind CDW and superconductivity. In CsV_3Sb_5, hole doping at the cesium site was achieved by oxidation of exfoliated thin flakes, enhancing the superconductivity and suppressing CDW order, suggesting competition between them [26]. A similar evolution of superconductivity and CDW order has also been observed in chemically hole-doped $Cs(V_{1-x}Ti_x)_3Sb_5$, $AV_3Sb_{5-x}Sn_x$, and isovalent-doped $Cs(V_{1-x}Nb_x)_3Sb_5$ [27–32]. Furthermore, a second superconducting dome was found with increased chemical doping [27,28]. On the electron doping side, dosing cesium on the surface of CsV_3Sb_5 can also suppress the CDW order [33], but the electron doping effect on superconductivity and its interplay with CDW remain unclear.

In this work, we explore the doping evolution of superconductivity, CDW order, and AHE in electron-doped $Cs(V_{1-x}Cr_x)_3Sb_5$ ($x = 0$, 1, 3, 6, 9, 15, 25%). High-quality $Cs(V_{1-x}Cr_x)_3Sb_5$ single crystals were synthesized via the self-flux method. The high-purity vanadium powder (Aladdin, 99.9%), antimony shot (Aladdin, 99.999%), and cesium liquid (Alfa Aesar, 99.98%) with the mole ratio of Cs : V : Cr : Sb = 1 : 1−x : x : 4 were mixed and loaded into an alumina crucible, and sealed in a quartz tube under vacuum. The sealed quartz tube was slowly heated to 1000 °C and soaked for 24 h. Subsequently, it was cooled to 900 °C at 100 °C/h and then to 650 °C at 1 °C/h. Once cooled to 650 °C, the excess flux was removed using a centrifuge, and shiny plate-like single crystals could be obtained. Due to the high reactivity of the starting materials, all preparation processes were conducted in an inert argon atmosphere.

II. EXPERIMENTAL DETAILS

The x-ray diffraction (XRD) measurements of the $Cs(V_{1-x}Cr_x)_3Sb_5$ single crystals were performed on a Bruker

*zhaoj@fudan.edu.cn

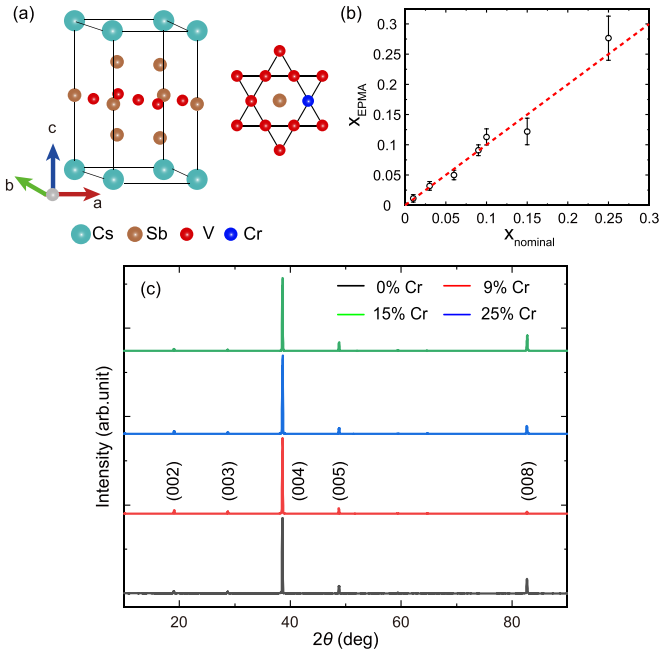

FIG. 1. (a) Crystal structure of $Cs(V_{1-x}Cr_x)_3Sb_5$. The vanadium/chromium atoms form the kagome lattice in the *ab* plane. (b) EPMA-measured chromium concentration versus nominal chromium concentration for the $Cs(V_{1-x}Cr_x)_3Sb_5$ single crystals. (c) X-ray diffraction pattern of $Cs(V_{1-x}Cr_x)_3Sb_5$ single crystals with $x = 0$, 9, 15, and 25%, respectively, showing only a series of $(00l)$ peaks.

D8 Discover diffractometer using Cu-K_α radiation with a monochrometer ($\lambda = 0.15418$ nm). The element analysis was conducted using an electron probe microanalyzer with the EPMA-1720/1720H instrument (Shimadzu) under an acceleration voltage of 15 kV, a beam current of 10 nA, and an electron beam size of 5 μm. Three different positions on the surface of each $Cs(V_{1-x}Cr_x)_3Sb_5$ single crystal were evenly selected and averaged to detect the actual chromium concentration. The dc magnetic susceptibility was measured using a SQUID magnetometer (MPMS3, Quantum Design). The heat capacity measurements were conducted using thermal relaxation methods on the Physical Properties Measurement System (PPMS, Quantum Design). The measurements for in-plane longitudinal resistivity and Hall resistivity were performed in four- and five-probe geometries on the PPMS, respectively, with a current of 3 mA flowing in the *ab* plane and a magnetic field applied along the *c*-axis. Silver paint and silver wire were used to make electrical contact to single crystals of $Cs(V_{1-x}Cr_x)_3Sb_5$. To eliminate the magnetoresistance component contribution in the Hall measurement, all the Hall resistivity data were antisymmetrized using the formula $\rho_{yx}(B) = [\rho_{yx}(+B) - \rho_{yx}(-B)]/2$.

III. RESULTS AND DISCUSSION

The crystal structure of $Cs(V_{1-x}Cr_x)_3Sb_5$ is shown in Fig. 1(a), where the vanadium atoms and chromium dopants form the kagome network. Figure 1(c) displays a series of XRD patterns of representative $Cs(V_{1-x}Cr_x)_3Sb_5$ single crystals with $x = 0$, 0.09, 0.15, 0.25, respectively (see Supplemental Material Fig. S1 [34] for all chromium-doping single crystals with x from 0 to 0.25). The data were shifted in intensity for clarity. All XRD patterns for our doped single crystals show only pronounced $(00l)$ diffraction peaks, and no impurity phases were detected (see Supplemental Material Fig. S1 [34]). The $(00l)$ peaks do not show a considerable shift with chromium doping, probably owing to the similar ionic radius of chromium and vanadium. A similar situation was also seen in niobium-doped $Cs(V_{1-x}Nb_x)_3Sb_5$ [30]. Furthermore, we conducted the powder XRD measurements on grounded $Cs(V_{1-x}Cr_x)_3Sb_5$ single crystals with a representative x value, and the data were refined with the Rietveld method using FullProf software. The refined results were summarized in Supplemental Material Fig. S2 and Table S1 [34]. The element analysis was carried out by electron probe microanalysis (EPMA) to estimate the actual chromium doping concentration of the $Cs(V_{1-x}Cr_x)_3Sb_5$ single crystals. The measured chromium concentration shows good homogeneity for different selected positions within each single crystal. The measured results are consistent with the nominal concentrations [Fig. 1(b)]. Next, we use the nominal compositions of chromium doping to label all compounds.

Superconductivity in the parent CsV_3Sb_5 is confirmed by the zero resistivity and diamagnetism below the superconducting transition temperature of $T_c \sim 3$ K [Figs. 2(b) and 2(d)]. T_c is rapidly suppressed to 1.6 K at $x = 0.03$, then entirely killed at higher doping. The rapid suppression of T_c with increasing chromium doping in $Cs(V_{1-x}Cr_x)_3Sb_5$ is distinct from the situation of hole-doped $Cs(V_{1-x}Ti_x)_3Sb_5$ [27,29], $AV_3Sb_{5-x}Sn_x$ [28,32], and isovalent-doped $Cs(V_{1-x}Nb_x)_3Sb_5$ [30,31], where T_c is enhanced by a small amount of chemical doping.

In the normal state above T_c, the resistivity of CsV_3Sb_5 exhibits a kink feature at ~94 K [Fig. 2(a)], indicative of the CDW transition. This is consistent with previous reports [2]. T_{CDW} shifts gradually from ~94 K for $x = 0$ to ~79 K for $x = 0.15$ and eventually vanishes for $x = 0.25$. A similar drop associated with the CDW transition is also seen in the temperature dependence of magnetic susceptibility in $Cs(V_{1-x}Cr_x)_3Sb_5$ [Fig. 2(c)]. The heat capacity of CsV_3Sb_5 also shows a sharp peak at $T_{CDW} \sim 94$ K, and the peak weakens and shifts to lower temperatures with increasing chromium concentration [Fig. 2(e)], which confirms the evolution of CDW order. Notably, the CDW order is fragile for hole doping cases and could be easily suppressed by a small percentage of hole doping [28,29,32]. However, in $Cs(V_{1-x}Cr_x)_3Sb_5$, the CDW is more robust against electron doping and survives at significantly higher doping concentrations (above 15%).

It has been shown that the AHE accompanies the CDW in CsV_3Sb_5 and related compounds [11–13,30]. Therefore, it is interesting to study the evolution of AHE in electron-doped $Cs(V_{1-x}Cr_x)_3Sb_5$, where the CDW order is gradually suppressed. For CsV_3Sb_5, the Hall resistivity ρ_{yx} exhibits an antisymmetric, sideways S line shape at low magnetic fields, indicating the presence of the AHE [Fig. 3(a)]. This is consistent with previous reports [11–13,30]. With increasing chromium doping, the antisymmetric, sideways S line shape feature becomes weaker [Figs. 3(b) and 3(e)]. Un-

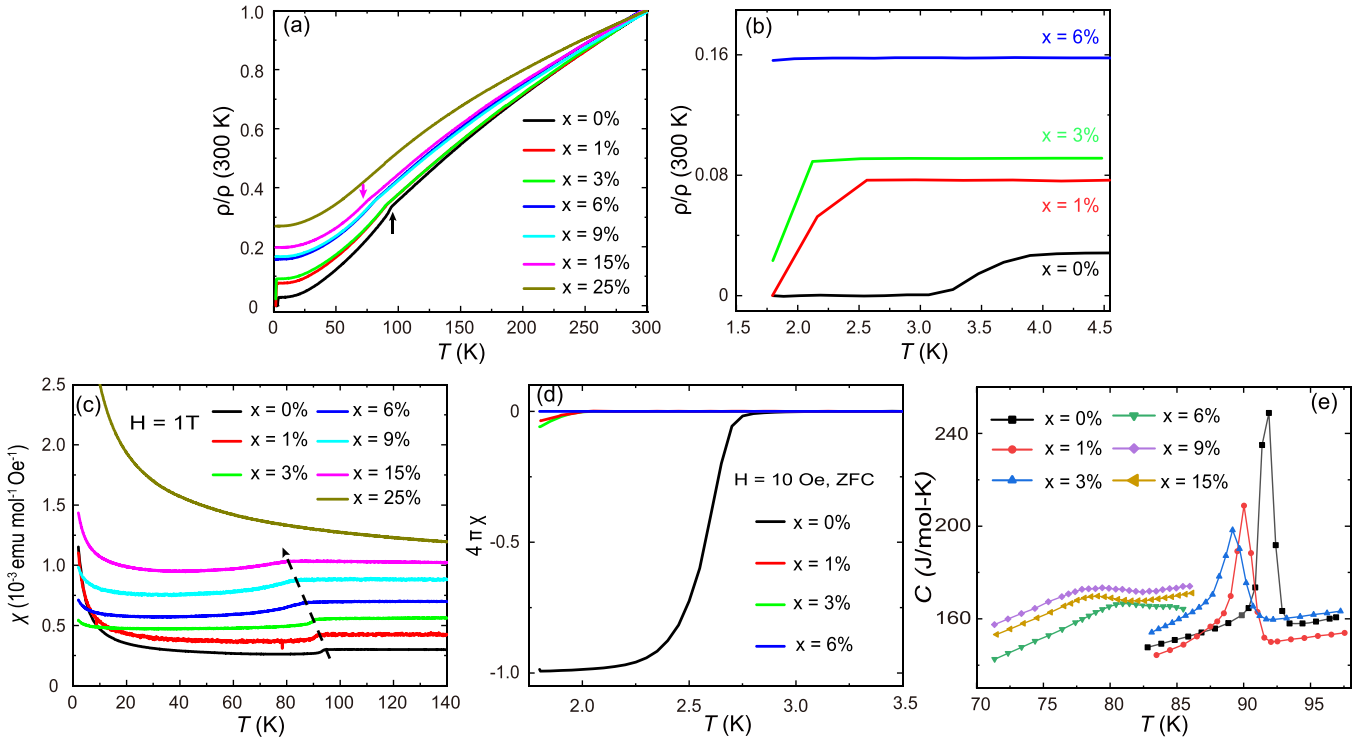

FIG. 2. (a) Temperature-dependent in-plane resistivity of $Cs(V_{1-x}Cr_x)_3Sb_5$ single crystals with x from 0 to 0.25. The data were normalized with respect to the resistivity at 300 K. The arrows indicate the CDW transition. (b) In the zoom-in low-temperature data of (a) near the superconductivity temperature, it is clear that T_c decreases monotonically with chromium doping. (c) Temperature dependence of magnetic susceptibility χ measured under zero-field-cooling (ZFC) conditions ($H = 1$ T, perpendicular to the c-axis). T_{CDW} shifts to lower temperatures with increasing chromium concentrations. (d) The temperature dependence of magnetic susceptibility was measured with an applied field of 10 Oe in the ab plane to show the evolution of T_c. (e) The temperature-dependent heat capacity at zero fields near the CDW transition.

like CsV_3Sb_5, where the sign change of the slope of ρ_{yx} appears at around 30 K, the slope of ρ_{yx} remains negative through the whole temperature range without a sign change for all doping levels of $Cs(V_{1-x}Cr_x)_3Sb_5$ [Figs. 3(b) and 3(e)]. This indicates the dominated electron carriers in chromium-doped samples. We extracted anomalous Hall resistivity (ρ_{yx}^{AHE}) at 5 K by subtracting the local linear ordinary Hall background [Fig. 3(f)]. It is shown that the anomalous Hall resistivity nearly vanishes at around $x = 0.06$, where the CDW order remains relatively strong. This implies that, in addition to CDW, other factors such as the detailed band structure may also play important roles in AHE.

Figure 4 summarizes the phase diagram of $Cs(V_{1-x}Cr_x)_3Sb_5$. It is evident that the introduction of chromium causes the rapid suppression of T_c, while the CDW order is relatively robust against chromium doping and survives at higher doping ($x = 0.15$). This is different from pressurized AV_3Sb_5 [35,36] and hole-doped $Cs(V_{1-x}Ti_x)_3Sb_5$/$CsV_3Sb_{5-x}Sn_x$ [27,28], which exhibit enhanced T_c and suppressed T_{CDW} in the low doping regime accompanied by a second superconducting dome at a high doping regime. We note that in the $CuIr_2Te_4$ superconductor accompanied by a CDW order, a magnetic order appears following the vanishing of superconductivity and CDW under chromium doping [37]. In $Cs(V_{1-x}Cr_x)_3Sb_5$, no magnetic order appeared up to the highest chromium doping level (25%), probably owing to the strong geometric frustration associated with the kagome lattice. It would be particularly interesting to understand the nature of magnetic correlations and their interplay with band topology in the high chromium doping regime in $Cs(V_{1-x}Cr_x)_3Sb_5$.

It has been suggested that the van Hove singularities (VHS) at the M point near the Fermi level plays a crucial role in the formation of the CDW order in CsV_3Sb_5 [26,28–30,35,38–42]. In a rigid-band shift approximation, isovalent and hole doping would push the VHS at the M point above the Fermi level and suppress the CDW order in $Cs(V_{1-x}Nb_x)_3Sb_5$ and $Cs(V_{1-x}Ti_x)_3Sb_5$ [29,30]. In the case of $Cs(V_{1-x}Cr_x)_3Sb_5$, chromium doping acts as an electron donor, and the VHS at the M point is expected to shift below the Fermi level. However, it was shown that the VHS at the M point exhibits dispersion along the k_z direction [39,40], and the VHS at the L point is above the Fermi level in CsV_3Sb_5 [29]. Therefore, when the Fermi level shifts upward under a small amount of chromium doping, the VHS at L would first approach the Fermi level, which may help stabilize the CDW order. This could explain the relatively robust CDW order against electron doping in $Cs(V_{1-x}Cr_x)_3Sb_5$. In the meantime, the Γ-centered antimony electron Fermi surface, which is believed to relate to superconductivity [29–31], expands with increased density of states under chromium doping. The rapid suppression of T_c in $Cs(V_{1-x}Cr_x)_3Sb_5$ cannot be readily explained by the enhanced density of states and suppressed CDW order. This

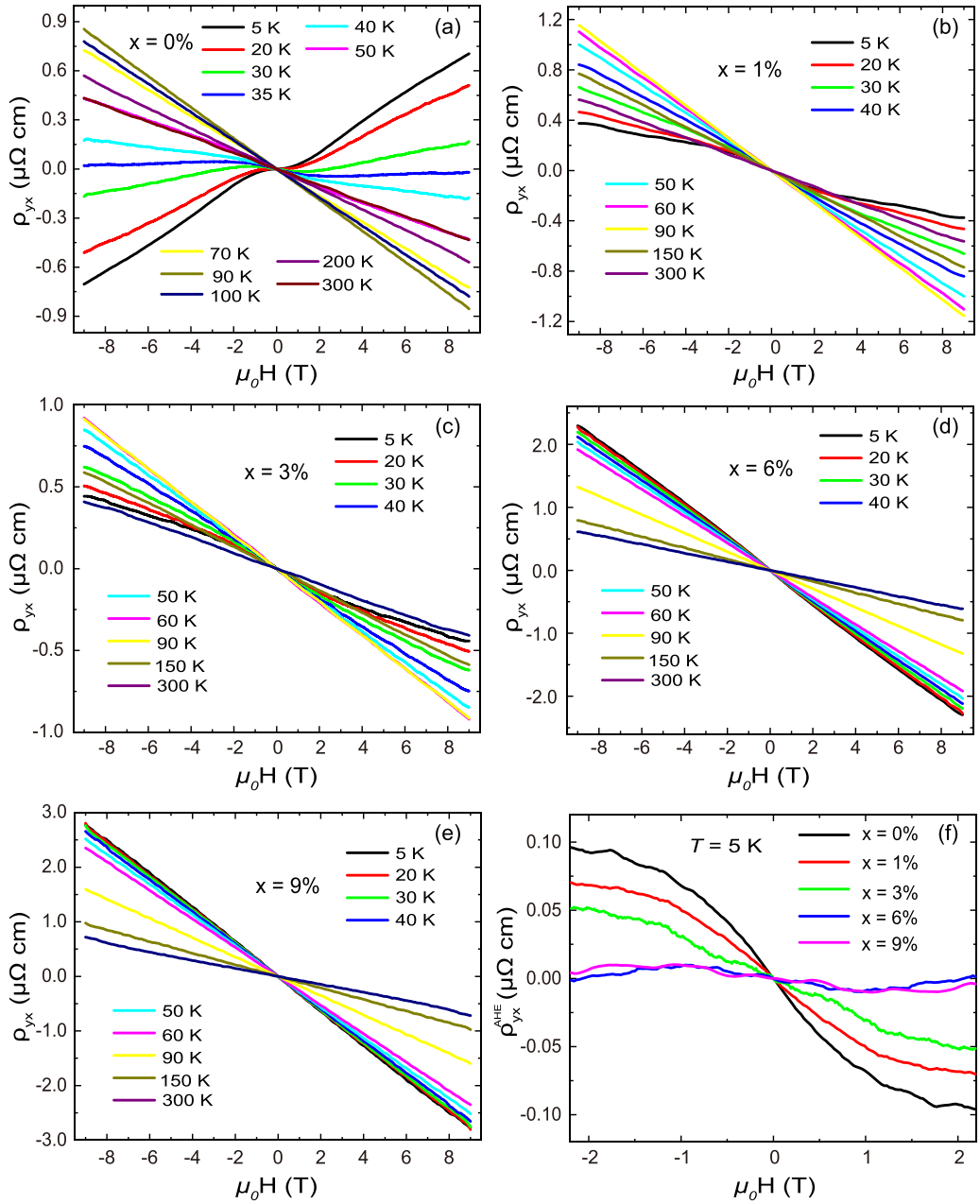

FIG. 3. (a)–(e) Field dependence of Hall resistivity at various temperatures for $Cs(V_{1-x}Cr_x)_3Sb_5$ ($x = 0$, 0.01, 0.03,0.06, 0.09) from 5 K to 300 K. (f) The extracted anomalous Hall resistivity (ρ_{yx}^{AHE}) by subtracting the local linear ordinary Hall background at 5 K for chromium doping content from $x = 0$ to $x = 0.09$. The Hall resistivity was measured using the five-probe method with the current flowing in the *ab* plane and a magnetic field applied along the *c*-axis.

suggests that, in addition to electron doping, chromium substitution may also introduce magnetic impurities that break the Cooper pair. Indeed, recent STM measurements have revealed an in-gap state with magnetic impurities in CsV_3Sb_5 [22]. These results therefore support the scenario of conventional *s*-wave pairing with no sign change.

IV. CONCLUSIONS

In summary, we have synthesized chromium-doped $Cs(V_{1-x}Cr_x)_3Sb_5$ single crystals with a controllable electron doping concentration and examined the evolution of the CDW and superconductivity. Unlike hole-doped CsV_3Sb_5, where the CDW is rapidly suppressed and superconductivity exhibits a double-dome feature, our experiment revealed that superconductivity is rapidly suppressed, and the CDW order is suppressed very slowly by chromium doping. The evolution of the CDW order could be understood through the band structure modifications by electron doping within the rigid-band approximation, suggesting the importance of VHS near *M* and *L* for the CDW order. In addition to electron doping, chromium substitution also introduces magnetic

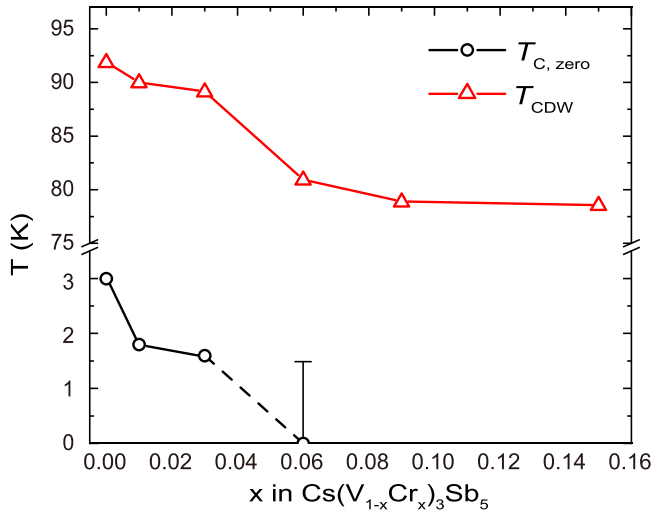

FIG. 4. The electron doping phase diagram of $Cs(V_{1-x}Cr_x)_3Sb_5$. The CDW ordering temperature is slowly suppressed to 79 K at $x = 15\%$ and further vanishes at $x = 25\%$. At the same time, T_c decreases monotonically with chromium doping and disappears at $x = 6\%$, where the error bar of T_c for $x = 0.06$ shows the possible lower superconducting transition temperature below 1.8 K. T_c was determined by the onset temperature of zero resistivity and T_{CDW} was determined by the heat capacity peak.

impurities that break the Cooper pair and suppress superconductivity. Our results support the scenario of a conventional sign-preserved *s*-wave pairing in this system.

Note added. During submission of this manuscript, we became aware of a work reporting molybdenum doping effects in $CsV_{3-x}Mo_xSb_5$, which exhibits suppressed superconductivity and enhanced CDW [43].

ACKNOWLEDGMENTS

We thank Dr. Di Yue for assistance with EPMA measurements. This work was supported by the Key Program of National Natural Science Foundation of China (Grant No. 12234006), the General Program of National Natural Science Foundation of China (Grant No. 11874119), the National Key R&D Program of China (Grant No. 2022YFA1403202), and the Shanghai Municipal Science and Technology Major Project (Grant No. 2019SHZDZX01). H. W. acknowledges support from the China National Postdoctoral Program for Innovative Talents (Grant No. BX2021080), China Postdoctoral Science Foundation (Grant No. 2020M700860), and Shanghai Post-doctoral Excellence Program (Grant No. 2021481).

[1] B. R. Ortiz *et al.*, Phys. Rev. Mater. **3**, 094407 (2019).
[2] B. R. Ortiz *et al.*, Phys. Rev. Lett. **125**, 247002 (2020).
[3] Q. Yin, Z. Tu, C. Gong, Y. Fu, S. Yan, and H. Lei, Chin. Phys. Lett. **38**, 037403 (2021).
[4] T. Neupert, M. M. Denner, J.- X. Yin, R. Thomale, and M. Z. Hasan, Nat. Phys. **18**, 137 (2021).
[5] T. Nguyen and M. Li, J. Appl. Phys. **131**, 060901 (2022).
[6] K. Jiang, T. Wu, J.-X. Yin, Z. Wang, M. Z. Hasan, S. D. Wilson, X. Chen, and J. Hu, National Sci. Rev. nwac199 (2022).
[7] Y. X. Jiang *et al.*, Nat. Mater. **20**, 1353 (2021).
[8] N. Shumiya *et al.*, Phys. Rev. B **104**, 035131 (2021).
[9] Z. Wang *et al.*, Phys. Rev. B **104**, 075148 (2021).
[10] C. Mielke, 3rd *et al.*, Nature (London) **602**, 245 (2022).
[11] S. Y. Yang *et al.*, Sci. Adv. **6**, eabb6003 (2020).
[12] F. H. Yu, T. Wu, Z. Y. Wang, B. Lei, W. Z. Zhuo, J. J. Ying, and X. H. Chen, Phys. Rev. B **104**, L041103 (2021).
[13] F.- H. Yu, X.- K. Wen, Z.- G. Gui, T. Wu, Z. Wang, Z.- J. Xiang, J. Ying, and X. Chen, Chin. Phys. B **31**, 017405 (2022).
[14] E. M. Kenney, B. R. Ortiz, C. Wang, S. D. Wilson, and M. J. Graf, J. Phys. Condens. Matter **33**, 235801 (2021).
[15] X. Feng, K. Jiang, Z. Wang, and J. Hu, Sci. Bull. **66**, 1384 (2021).
[16] X. Feng, Y. Zhang, K. Jiang, and J. Hu, Phys. Rev. B **104**, 165136 (2021).
[17] M. M. Denner, R. Thomale, and T. Neupert, Phys. Rev. Lett. **127**, 217601 (2021).
[18] C. C. Zhao *et al.*, arXiv:2102.08356.
[19] W. Duan *et al.*, Sci. China Phys. Mech. Astron. **64**, 107462 (2021).
[20] C. Mu, Q. Yin, Z. Tu, C. Gong, H. Lei, Z. Li, and J. Luo, Chin. Phys. Lett. **38**, 077402 (2021).
[21] C. Mu, Q. Yin, Z. Tu, C. Gong, P. Zheng, H. Lei, Z. Li, and J. Luo, Chin. Phys. B **31**, 017105 (2022).
[22] H. S. Xu, Y. J. Yan, R. Yin, W. Xia, S. Fang, Z. Chen, Y. Li, W. Yang, Y. Guo, and D. L. Feng, Phys. Rev. Lett. **127**, 187004 (2021).
[23] L. Nie *et al.*, Nature (London) **604**, 59 (2022).
[24] Y. Xiang, Q. Li, Y. Li, W. Xie, H. Yang, Z. Wang, Y. Yao, and H. H. Wen, Nat. Commun. **12**, 6727 (2021).
[25] Z. Liang *et al.*, Phys. Rev. X **11**, 031026 (2021).
[26] Y. Song, T. Ying, X. Chen, X. Han, X. Wu, A. P. Schnyder, Y. Huang, J. G. Guo, and X. Chen, Phys. Rev. Lett. **127**, 237001 (2021).
[27] H. Yang *et al.*, arXiv:2110.11228.
[28] Y. M. Oey, B. R. Ortiz, F. Kaboudvand, J. Frassineti, E. Garcia, R. Cong, S. Sanna, V. F. Mitrović, R. Seshadri, and S. D. Wilson, Phys. Rev. Mater. **6**, L041801 (2022).
[29] Y. Liu *et al.*, arXiv:2110.12651.
[30] Y. Li *et al.*, Phys. Rev. B **105**, L180507 (2022).
[31] T. Kato *et al.*, Phys. Rev. Lett. **129**, 206402 (2022).
[32] Y. M. Oey, F. Kaboudvand, B. R. Ortiz, R. Seshadri, and S. D. Wilson, Phys. Rev. Mater. **6**, 074802 (2022).
[33] K. Nakayama, Y. Li, T. Kato, M. Liu, Z. Wang, T. Takahashi, Y. Yao, and T. Sato, Phys. Rev. X **12**, 011001 (2022).
[34] See Supplemental Material at http://link.aps.org/supplemental/10.1103/PhysRevB.106.235151 for details of single-crystal XRD, powder XRD, and refinement results for $Cs(V_{1-x}Cr_x)_3Sb_5$.
[35] K. Y. Chen *et al.*, Phys. Rev. Lett. **126**, 247001 (2021).
[36] F. H. Yu, D. H. Ma, W. Z. Zhuo, S. Q. Liu, X. K. Wen, B. Lei, J. J. Ying, and X. H. Chen, Nat. Commun. **12**, 3645 (2021).
[37] L. Zeng *et al.*, J. Phys. Chem. Lett. **13**, 2442 (2022).

[38] H. LaBollita and A. S. Botana, Phys. Rev. B **104**, 205129 (2021).
[39] Y. Hu *et al.*, Nat. Commun. **13**, 2220 (2022).
[40] M. Kang *et al.*, Nat. Phys. **18**, 301 (2022).
[41] H. Tan, Y. Liu, Z. Wang, and B. Yan, Phys. Rev. Lett. **127**, 046401 (2021).
[42] X. Zhou, Y. Li, X. Fan, J. Hao, Y. Dai, Z. Wang, Y. Yao, and H.- H. Wen, Phys. Rev. B **104**, L041101 (2021).
[43] M. Liu, T. Han, X. Hu, Y. Tu, Z. Zhang, M. Long, X. Hou, Q. Mu, and L. Shan, Phys. Rev. B **106**, L140501 (2022).